Acta Neuropathol (2012) 123:85–96
DOI 10.1007/s00401-011-0929-5

ORIGINAL PAPER

Entorhinal verrucae geometry is coincident and correlates with Alzheimer's lesions: a combined neuropathology and high-resolution ex vivo MRI analysis

Jean C. Augustinack · Kristen E. Huber · Gheorghe M. Postelnicu · Sita Kakunoori · Ruopeng Wang · André J. W. van der Kouwe · Lawrence L. Wald · Thor D. Stein · Matthew P. Frosch · Bruce Fischl

Received: 30 September 2011 / Revised: 5 December 2011 / Accepted: 6 December 2011 / Published online: 13 December 2011

Abstract Entorhinal cortex displays a distinctive organization in layer II and forms small elevations on its surface called entorhinal verrucae. In Alzheimer's disease, the verrucae disappear due to neurofibrillary tangle formation and neuronal death. Isosurface models were reconstructed from high-resolution ex vivo MRI volumes scanned at 7.0 T and individual verruca were measured quantitatively for height, width, volume, and surface area on control and mild Alzheimer's cases. Mean verruca height was 0.13 ± 0.04 mm for our cognitively normal (controls) sample set whereas for mild AD samples mean height was 0.11 mm $\pm$ 0.05 mm ($p < 0.001$) in entorhinal cortex ($n = 10$ cases). These quantitative methods were validated by a significant correlation of verrucae height and volume with qualitative verrucae ratings ($n = 36$ cases). Entorhinal surfaces were significantly different from other cortical heights such as, cingulate, frontal, occipital, parietal and temporal cortices. Colocalization of verrucae with entorhinal islands was confirmed in ex vivo MRI and, moreover, verrucae ratings were negatively correlated to Braak and Braak pathological stage. This study characterizes novel methods to measure individual entorhinal verruca size, and shows that verrucae size correlates to Alzheimer's pathology. Taken together, these results suggest that verrucae may have the potential to serve as an early and specific morphological marker for mild cognitive impairment and Alzheimer's disease.

Keywords Neuroimaging · Modularity · Cortex · Ex vivo · Surface reconstruction

J. C. Augustinack (✉) · K. E. Huber · S. Kakunoori · R. Wang · A. J. W. van der Kouwe · L. L. Wald · B. Fischl
Department of Radiology, Athinoula A. Martinos Center for Biomedical Imaging, Massachusetts General Hospital, Building 149–13th St., Room 2301, Charlestown, MA 02129, USA
e-mail: jean@nmr.mgh.harvard.edu

G. M. Postelnicu
Google, Inc., 110 Brandschenkestrasse, 8002 Zurich, Switzerland

T. D. Stein · M. P. Frosch
Department of Neuropathology, Massachusetts General Hospital, 55 Fruit St., Boston, MA 02115, USA

B. Fischl
CSAIL, MIT, 32 Vassar Street, Cambridge, MA 02139, USA

Introduction

The reliability of memory depends on an intact neuroanatomical system in the medial temporal lobe that includes entorhinal cortex and hippocampus [12, 51]. In Alzheimer's disease (AD), neurons in the entorhinal cortex, particularly those in layer II, begin to die and some leave behind a pathological marker—the neurofibrillary tangle (NFT) [27, 29]. NFTs and significant cell death characterize the neuronal loss in AD where NFTs and subsequent atrophy have been correlated with dementia [2, 19, 41]. The presence of NFTs and concomitant neuronal death represent a disease-related process and not an age-related decline [21, 26].

In many human brains, entorhinal layer II bulges out on the entorhinal surface and causes small bumps, presumably due to large neuronal cell bodies beneath [46, 52]. Although anatomists described them as 'hippocampi verrucae' a century ago [30, 40], few reports since then have studied the verrucae. Simic and colleagues [43] described that the number of entorhinal verrucae increased with age and that overall verrucae area decreased during aging.

Solodkin and Van Hoesen [44] correlated verrucae destruction to AD in pathological specimens. Thus, in AD, entorhinal cortex undergoes massive atrophy and the entorhinal verrucae disappear. The demise of entorhinal cortex and hippocampal CA1 has been correlated to mild cognitive impairment [9, 26] and this suggests that the destruction of entorhinal layer II occurs at or before mild cognitive impairment when therapeutic effects can be most beneficial. Since NFTs in entorhinal layer II lie directly underneath entorhinal verrucae, the verrucae represent a presumptive morphological neuroimaging marker for AD.

Recent advances in MRI have allowed detection of cytoarchitectural features in the human brain [7, 13] and in particular entorhinal layer II in high-resolution (100 μm^3) ex vivo MRI [4]. To determine the individual verruca size, we developed an algorithm to measure height, volume, surface area and width on isosurface reconstructions from our medial temporal lobe ex vivo MRI. Our results confirm that entorhinal cortex surface differs from other cortical surfaces, and that a 3D spatial relationship exists between entorhinal islands and entorhinal verrucae as observed in ex vivo MRI. Moreover, we found that verrucae from mild AD cases were smaller than normal control surfaces in entorhinal cortex, and that verrucae size correlated to Braak and Braak staging. This model elucidates the magnitude of entorhinal verrucae in normal controls and AD and relates their size to disease severity. These results demonstrate a significant correlation between entorhinal verrucae size and AD pathology and points to a specific morphological marker in normal controls and mild AD.

Methods

Brain samples

Thirty-six entorhinal cortex samples were obtained from the Massachusetts General Hospital Alzheimer's Disease Research Center or Massachusetts General Hospital Autopsy Service. In addition, we obtained eight additional cortical samples (motor, occipital, fusiform, Wernicke's, frontal, cingulate) that we imaged to serve as a surface control (i.e., not diagnostic control) to show verrucae are unique to entorhinal cortex, and to validate our quantitative model. Most of the neocortical and cingulate samples were obtained from the same control cases as medial temporal samples. Samples were either fixed with 10% formalin from Autopsy Service or 4% paraformaldehyde from our Alzheimer's Disease Research Center for at least 2 weeks. Postmortem interval was less than 48 h and samples included 20 males, 14 females, 2 with gender information unavailable, with age ranging from 43 to 102 years (mean 76 years). We further describe demographic and diagnosis information in Table 1. Clinical diagnoses listed in Table 1 were received from the Memory Disorders Unit in Department of Neurology at the Massachusetts General Hospital. Non-Alzheimer's dementias were excluded from this study. Of the 36 entorhinal samples, all were evaluated for verrucae rating assay ($n = 36$), but a subset of this group was examined for the verrucae metric assay ($n = 10$).

Table 1 Demographic and diagnostic information for the cases studied

Case	Age	Sex	Hemi	PMI (h)	Neuropath Dx	Clinical Dx
1 a	n/a	F	LH	<24	Control	Control
2 a	68	M	RH	<24	Control	Control
3 a	43	F	LH	<24	Control	Control
4 a	65	M	LH	25	Control	Control
5 a	67	M	RH	12	Control	Control
6 a	50	F	RH	16	Control	Control
7	61	M	n/a	7.5	Control	Control
8	68	M	LH	n/a	Control	Control
9	61	M	LH	22	AD, B&B I	Control
10 a	n/a	n/a	LH	<24	AD, B&B I	Control
11 a	60	M	RH	<24	AD, B&B I	Control
12 a	n/a	n/a	LH	<24	AD, B&B II	Control
13	95	M	RH	20	AD, B&B III	Control
14 a	86	F	LH	18	AD, B&B III	AD
15	79	F	LH	6	AD, B&B III	AD
16	87	M	RH	n/a	AD, B&B III	AD
17	87	M	LH	48	AD, B&B IV	AD
18	82	F	RH	12	AD, B&B IV	AD
19	89	M	RH	14	AD, B&B IV	AD
20	84	M	RH	10	AD, B&B V	AD
21	90	F	RH	24	AD, B&B V	AD
22	93	F	RH	15	AD, B&B V	AD
23	77	M	LH	48	AD, B&B V	AD
24	102	M	n/a	n/a	AD, B&B V	AD
25	90	F	RH	12	AD, B&B V	AD
26	92	F	RH	8	AD, B&B V	AD
27	73	M	RH	24	AD, B&B VI	AD
28	89	M	LH	22	AD, B&B VI	AD
29	69	M	RH	7	AD, B&B VI	AD
30	83	M	RH	22	AD, B&B VI	AD
31	87	M	LH	6	AD, B&B VI	AD
32	58	F	RH	17	AD, B&B VI	AD
33	90	M	LH	<12	AD, B&B VI	AD
34	81	F	RH	24	AD, B&B VI	AD
35	56	F	LH	7	AD, B&B VI	AD
36	60	F	LH	n/a	AD, B&B VI	AD

All cases have verrucae rating assessment and letter (a) denotes cases that have additional quantitative verrucae measurements

AD Alzheimer's disease, *B&B* Braak and Braak stage, *n/a* not available, *PMI* postmortem interval

Image acquisition

Images were collected on a 7.0-T whole body MRI scanner based on a Siemens Magnetom platform (Siemens Medical Systems, Erlangen, Germany) using a solenoid coil (28.5 mm i.d. × 44 mm in length, 4 turn). A conventional fast-low-angle-shot (FLASH) sequence was used with a resolution of 100 μm isotropic, field of view = 52 mm (512 × 512 matrix), slab thickness = 25.6 mm (256 partitions), TR = 20 ms, TE = 7.8 ms, bandwidth = 134 Hz/pixel, scan duration = 43 min 41 s, full Fourier encoding [4]. We have further optimized the MRI parameters, but maintained 100 μm^3 resolution, and acquired images with TR = 54 ms, TE = 25 ms, bandwidth = 30 Hz/pixel, 650 × 440 matrix that improved signal-to-noise ratio. Images were acquired with flip angles 10°, 20° and 30° and three FLASH images were averaged to generate a mean for each flip angle. In a subset of cases ($n = 10$), samples were scanned in hydrogen-free Fomblin (Solvay, Houston, TX, USA) in order to generate a clean surface reconstruction without surrounding liquid necessary for verrucae quantitative measurements. Gross photographs were captured with a Canon EOS Digital Rebel XT (8 MP) with a 50-mm lens.

Isosurface reconstruction

Three-dimensional isosurfaces of the entorhinal cortex were reconstructed from the MR volume with two different software packages to test reliability of our method. We used Freeview (Freeview, a visualization tool that is part of the FreeSurfer package, http://www.surfer.nmr.mgh.harvard.edu) and Amira (Amira, Berlin, Germany) to generate isosurfaces of entorhinal cortex and other cortices that were examined. In both, the cortical surface extraction was automated [14] and entorhinal surfaces were reconstructed from FLASH images at 100 μm^3 resolution with 20° flip angle. Although the visualization tools in Freeview and Amira implement different volume rendering schemes, both produced satisfactory isosurfaces. For convenience with our Linux-based MRI volumes, we used Freeview for all measurements in this report. Throughout this report, we use the terms isosurface and surface interchangeably.

Quantitative and qualitative verrucae surface assays

Quantitative surface assay

We selected verrucae that were measured using a systematic random sampling method. We used a transparent grid overlay that was 6 × 5 squares (30 total squares) and the overall grid measured 13.5 cm × 11.25 cm. Each individual box or square was 2.25 cm × 2.25 cm and had exclusion lines (bottom and left) and inclusion lines (top and right). Each surface reconstruction was zoomed so that the total grid (30 squares) covered the entorhinal surface at approximately the level of the amygdala where the grid was overlaid with the top aligned at the medial border of EC (nearly parallel with the hippocampal fissure) in every case. Visibly identifiable verrucae were labeled within each randomly selected grid square (i.e., we did not label random non-verrucae patches). We used a random number generator to determine which ten counting squares to label per case. Each case required approximately 30 min for manual labeling. This procedure generated a verrucae sample size, $n = 165$, for the quantitative verrucae measurements. Next, we analyzed the labels (or patches) with our 'verrucae metric' algorithm in MATLAB (MATLAB, MathWorks, Natick, MA, USA) that computed the optimal least-squares fitting plane at the base of the surface, and then measured for height, width, volume, and surface area of each surface patch. Height measurements were determined as the maximum perpendicular distance from the fitted plane at the base of the verruca to the isosurface (see schemata in Fig. 3d). Width was determined as the maximum diameter of the label and surface area was calculated as the sum of labeled triangles. Volume measures the space above the base-fitting plane and was computed as the sum volumes of the polyhedra obtained by projecting each of the surface triangles onto the base fitting plane. We obtained very slight differences in verrucae measurements between Amira and Freeview and attribute this variation to the different tessellation algorithms employed by each software package. These differences were not significant when compared using an independent samples t test.

Qualitative surface rating

Verrucae surface reconstructions were validated with photography of gross brains and a qualitative verrucae rating scale was developed for reliability. The qualitative rating protocol was created to assess verrucae magnitude in graded categories. The verrucae rating protocol consisted of 5 ranking categories: 1 = no verrucae (flat surface), 2 = verrucae are barely visible and very small, 3 = a few small and medium-sized verrucae are present, 4 = many small and medium size verrucae are present and finally 5 = several large prominent verrucae are present. Examples illustrate each rating category through gross photographs (Fig. 1). We developed the qualitative scale not only to establish reliability but also to avoid placing Alzheimer's Disease Research Center cases in Fomblin. Two raters (rater #1 = JCA and rater #2 = KEH) evaluated photographs for qualitative verrucae assessment and ratings were averaged for overall mean.

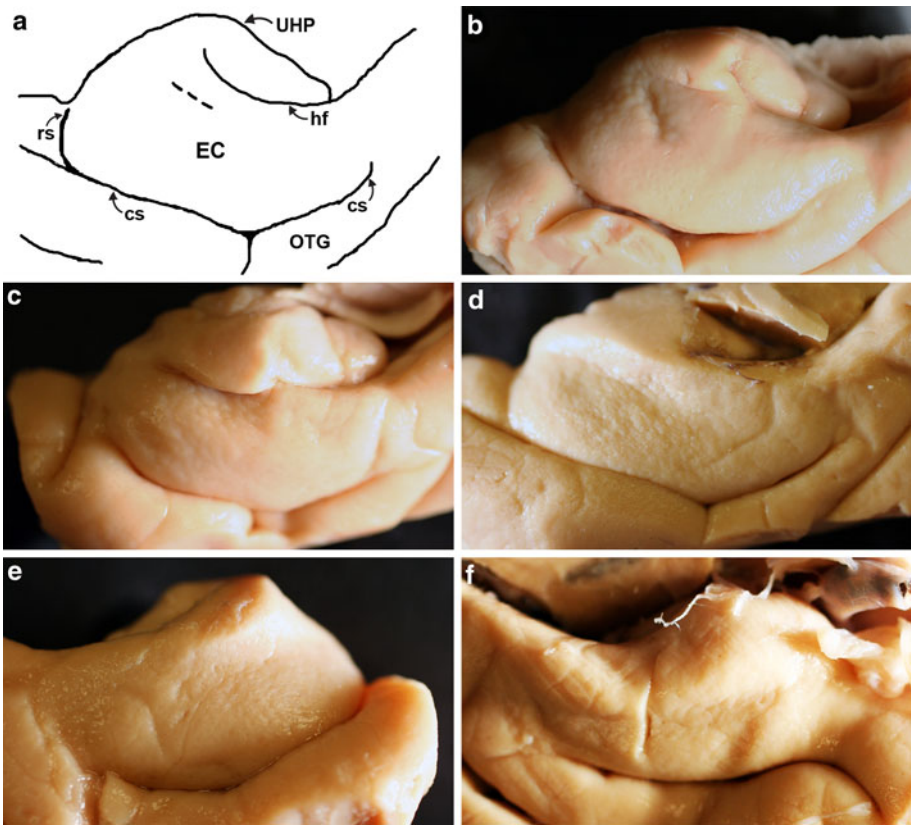

Fig. 1 Five qualitative categories demonstrate verrucae ratings in photographs. A drawing to outline medial temporal surface anatomy in (**a**). Rating 5 = several large prominent verrucae are present in (**b**), rating 4 = many small and medium size verrucae are present in (**c**), 3 = a few small and medium sized verrucae are present in (**d**), 2 = verrucae are barely visible and very small in (**e**), 1 = no verrucae (flat surface) in (**f**). Short-dotted line in (**a**) represents tentorial notch. *EC* entorhinal cortex, *cs* collateral sulcus, *hf* hippocampal fissure, *rs* rhinal sulcus, *OTG* occipitotemporal gyrus, *UHP* uncal hippocampus

Neuropathology analysis

All cases were stained with Nissl (thionin) for healthy cell bodies and thioflavine S to assess the presence of neurofibrillary tangles and senile plaques. Nissl staining was performed as previously published [4] and thioflavine S was performed according to Van Hoesen [55]. In brief, Nissl stains were pretreated and defatted. Subsequently, the sections were stained with 0.5% aqueous thionin for 5 min. Slides were dehydrated in ascending ethanol series, cleared in xylene and coverslipped with Permount (Fisher, Fair Lawn, NJ, USA). Thioflavine S sections were defatted and stained in 0.2% solution of Thioflavine S (Sigma, St. Louis, MO, USA) and coverslipped with water soluble mounting media. Additionally, Alzheimer's pathology was assessed using Rabbit anti-human tau (Dako, Carpinteria, CA, USA) and Bielschowsky's silver stain at MGH Department of Neuropathology. A standard immunocytochemical protocol was used with bovine serum albumin for blocking non-specific binding, primary antibody (anti-tau) dilution was 1/3,000 and visualized with 3′,3-Diaminobenzidine Peroxidase Substrate Kit (Vector, Burlingame, CA, USA). Bielschowsky's silver stain was adopted from University of Massachusetts Medical Center (Worcester, MA, USA). Alzheimer's disease and subsequent Braak and Braak staging was diagnosed and evaluated by neuropathologist (M.P.F. or T.S.) and J.C.A. at Massachusetts General Hospital. Braak and Braak staging determined the severity of neurofibrillary tangles in distinct and cumulative cortices. In brief, each stage is summarized, stage I represents neurofibrillary tangles in perirhinal cortex (layer II–III), stage II displays neurofibrillary tangles in entorhinal cortex (layer II), stage III adds entorhinal layer IV and CA1, stage V includes all hippocampal CA fields and subiculum and finally stage VI occurs when neocortical areas and dentate gyrus contain neurofibrillary tangles [10]. Cytoarchitecture and neuropathology were evaluated using a fluorescence Nikon 80i microscope (MVI, Avon, MA, USA).

Statistical analysis

Non-parametric correlations (Spearman's ρ) were used for qualitative–quantitative reliability tests and to compare verrucae rating with Braak and Braak stage. Mann–Whitney *U* test was used to compare other cortical surfaces to entorhinal cortex. Mann–Whitney *U* test was also used to compare verrucae rating with gender, and to compare quantitative and qualitative verrucae measures between control and AD cases. Cohen's Kappa was used to assess inter-rater reliability on qualitative verrucae ratings. *p* value was set at $p < 0.05$ for significance. Statistics were performed using SPSS (SPSS, IBM Corporation, Somers, NY, USA).

Results

Colocalization in MRI between EC islands and verrucae

From ex vivo MRI volumes of medial temporal lobe samples, we created surface reconstructions and found that entorhinal islands (layer II) colocalized with surface verrucae (labeled in blue) in all cases that showed visible islands and verrucae (i.e., most control cases). Each 2D image is shown with a partial surface reconstruction in coronal, sagittal and axial planes (Fig. 2a, b, c). In fast-low-angle-shot (FLASH) images in ex vivo MRI, bright intensities signify cell dense regions such as entorhinal islands in layer II. Islands were observed as spherical intensities in all views (Fig. 2). These data confirm the spatial relationship between entorhinal islands in layer II and surface elevations and adds a 3D modularity.

Surface reconstructions validate gross morphometry

We examined surface reconstructions of entorhinal cortex in normal control and Alzheimer's samples and found that our surface model (Fig. 3b) validates what was observed in the gross specimen (Fig. 3a). In fact, we found that the surface reconstruction improved detection of verrucae. We observed that the surface reconstructions yielded better visualization because the reconstruction improved shadowing that highlighted individual verruca and we had the ability to manually rotate the surface to illuminate all angles while evaluation with the gross photographs required more than one photo. A cognitively normal brain with entorhinal verrucae is illustrated in Fig. 3 to show the pipeline of our model. We labeled all individual verrucae on the entorhinal surface to show the extent of verrucae in a cognitively normal case (Fig. 3c). Blue labels highlight individual verruca where entorhinal verrucae were primarily observed at the level of the amygdala and hippocampal head and to a lesser extent at posterior levels. We developed code to quantitatively evaluate the size of an individual verruca. An individual verruca schemata is shown in Fig. 3d where height, width and surface area were measured and volume was calculated. The blue label in Fig. 3c corresponds to blue label in the diagram (Fig. 3d).

Quantitative differences in verrucae geometry between mild AD and controls

To further characterize the entorhinal verrucae, we labeled randomly selected verrucae in each case. For the quantitative measures, we found that normal control brains ($n = 6$; 100 labels) produced a verrucae height of 0.13 $\pm$ 0.04 mm (mean $\pm$ SD), verrucae width of 1.26 $\pm$ 0.29 mm (mean $\pm$ SD), verrucae surface area of 0.81 $\pm$ 0.37 mm^2 (mean $\pm$ SD) and verrucae volume of 0.05 $\pm$ 0.04 mm^3 (mean $\pm$ SD) (Table 2). The measured verrucae size for mild AD cases ($n = 4$; 65 labels) for verrucae height was 0.11 $\pm$ 0.05 mm (mean $\pm$ SD), verrucae width was 1.14 $\pm$ 0.22 mm (mean $\pm$ SD), verrucae surface area was 0.70 $\pm$ 0.30 mm^2 (mean $\pm$ SD) and finally verrucae volume was 0.04 $\pm$ 0.03 mm^3 (mean $\pm$ SD) (Table 2). We compared these verrucae measurements between normal controls ($n = 100$ verrucae, per metric) and mild AD cases ($n = 65$ verrucae, per metric) and found that verrucae height (Mann–Whitney U test, $p < 0.001$), width (Mann–Whitney U test, $p < 0.05$), surface area (Mann–Whitney U test, $p < 0.05$), and volume (Mann–Whitney U test, $p < 0.01$) were significantly decreased in the mild AD cases compared to normal controls. In sum, the reconstructed verrucae resembled those visually observed in the gross brain and verrucae quantitative measures showed a significant change in mild AD compared to controls.

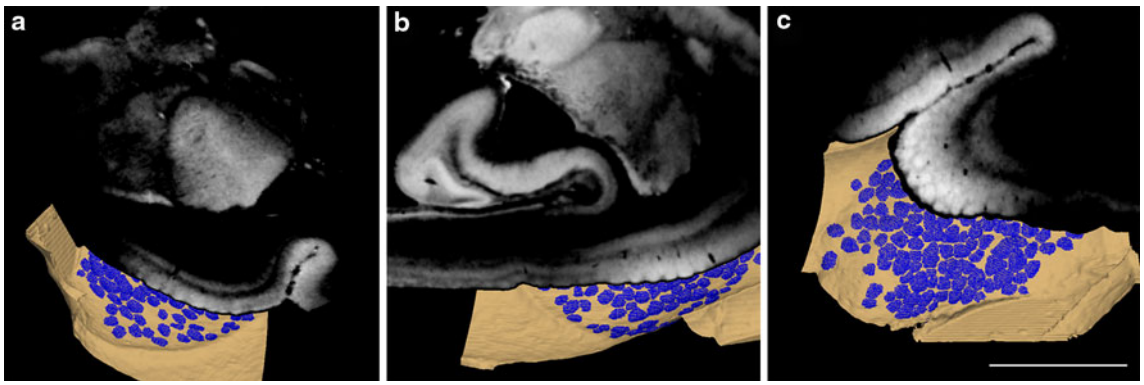

Fig. 2 Entorhinal cortex surface reconstructions with labeled verrucae (*blue*) shown with corresponding coronal (**a**), sagittal (**b**), and axial (**c**) MR images of medial temporal lobe. Note that that entorhinal islands (*bright spots*) on the MRI colocalize with labeled entorhinal verrucae (*blue*) on the surface. *Magnification bar* 1 cm

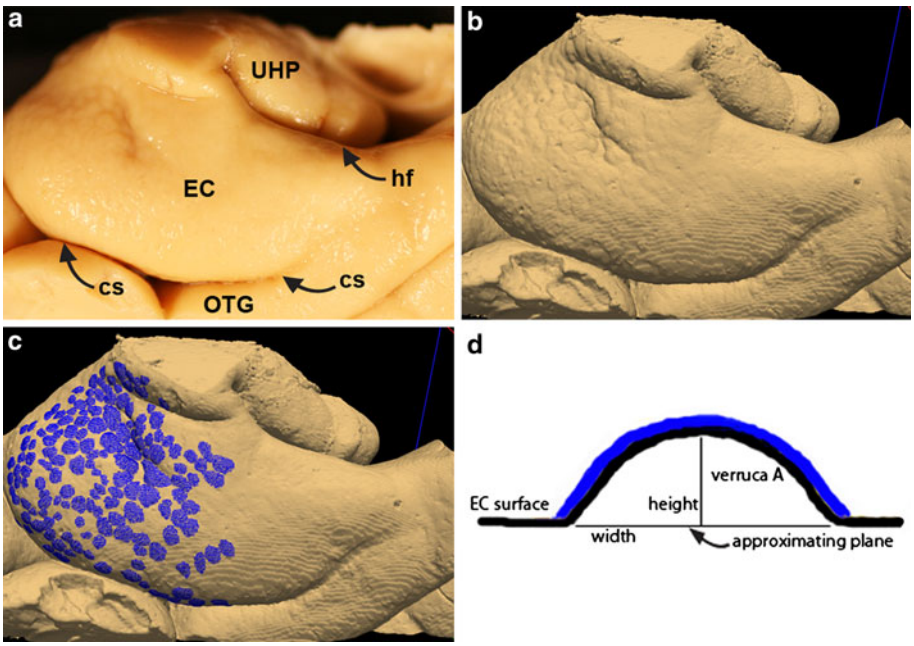

Fig. 3 Gross brain showing anterior parahippocampal gyrus (**a**) corresponds to 3D isosurface reconstruction from ex vivo MRI (**b**) in same case. Both the gross specimen and MRI reconstruction show entorhinal verrucae (labeled in *blue* in **c**) on the surface of the entorhinal cortex. Schemata of single verruca (**d**) shows label and algorithm metrics used to derive verrucae measurements. *EC* entorhinal cortex, *cs* collateral sulcus, *hf* hippocampal fissure, *OTG* occipitotemporal gyrus, *UHP* uncal hippocampus

Table 2 Quantitative verrucae measurements—height, width, surface area and volume—for entorhinal cortex surface compared between controls and mild Alzheimer's tissue samples

Diagnosis $n = 10$	EC verrucae height (mm)		EC verrucae width (mm)		EC verrucae surface area (mm^2)		EC verrucae volume (mm^3)	
	Mean	SD	Mean	SD	Mean	SD	Mean	SD
Controls	0.13	0.04	1.26	0.29	0.81	0.37	0.05	0.04
AD	0.11[a]	0.05	1.14[a]	0.22	0.70[a]	0.30	0.04[a]	0.03

[a] Significant difference from controls

Entorhinal surface significantly different from other cortical surfaces

To corroborate our measurement model, we imaged eight additional sample blocks from various other cortices and modalities such as, cingulate, frontal, occipital, parietal, temporal and motor. Since visible verrucae were not present in neocortical samples, we modeled our labels after the approximate width of our EC verrucae data to reproduce similar sized patches. We reconstructed the surfaces and randomly selected labels using the same methods as above and we found that these cortical surfaces were significantly different from entorhinal cortex in height. All heights were constrained to positive numbers and we restricted our samples and measurements to gyri (i.e., crowns) to control for overall geometry. Entorhinal heights ($n = 6$ cases, $n = 100$ labels) averaged 0.13 mm whereas motor, occipital, fusiform and Wernicke's area were all below 0.10 mm for height (i.e., motor cortex height 0.07 mm); $p < 0.001$, Mann–Whitney U test, for all non-entorhinal surfaces when compared to entorhinal) (Fig. 4), indicating a significantly flatter cortical surface in the control regions. Thus, entorhinal surfaces show significant differences from other neocortical tissue and demonstrate a more rugged topography compared to other cortical areas.

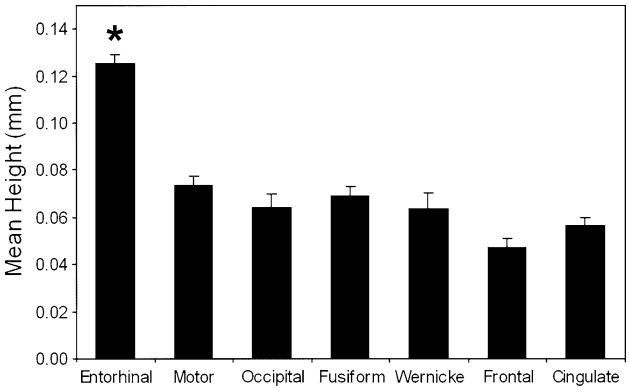

Fig. 4 Mean entorhinal verrucae height measures from six control cases (0.13 mm) were significantly higher than mean height of other cortices [motor cortex ($p < 0.001$), occipital ($p < 0.001$), fusiform ($p < 0.001$), Wernicke's ($p < 0.001$), frontal ($p < 0.001$) and cingulate ($p < 0.001$)]. These cortical regions were measured as a control surface and all heights measured less than 0.10 mm. *Asterisk* represents significant difference between entorhinal and other cortices. *Error bars* represent standard error

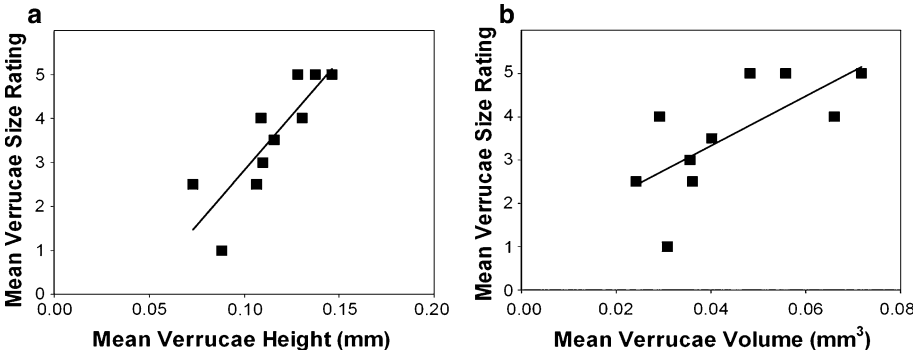

Fig. 5 Mean verrucae height was significantly positively correlated (Spearman's $\rho = 0.883$, $p < 0.01$, $n = 10$) with mean verrucae ratings (**a**) showing reliability of our quantitative methods. Mean verrucae volume was also significantly positively correlated (Spearman's $\rho = 0.716$, $p < 0.05$, $n = 10$) with mean verrucae ratings (**b**). Validation of the qualitative verrucae ratings with quantitative verrucae measures provides evidence of the accuracy of our entorhinal verrucae measurements

Verrucae qualitative ratings correlate with verrucae height and volume

As a supplement to quantitative verrucae measurements, we also developed a qualitative rating scale for reliability and to avoid scanning all cases in Fomblin liquid. Fomblin is a proton-free liquid used to minimize background effects and helped to generate a clean isosurface. The rating scale (described in methods) ranges from 1 to 5 where rating 1 denotes a flat surface and 5 indicates several large verrucae. We found that the quantitative measurements, height and volume, reconciled well with our qualitative rating scale and showed a significant positive correlation for height (Spearman's $\rho = 0.883$, $p < 0.01$, $n = 10$) and volume (Spearman's $\rho = 0.716$, $p < 0.05$, $n = 10$) (Fig. 5). Width and surface area measurements did not achieve significance compared to verrucae rating (width: Spearman's $\rho = 0.469$, $p = 0.17$, $n = 10$ and surface area: Spearman's $\rho = 0.519$, $p = 0.13$, $n = 10$).

Inter-rater reliability

We examined qualitative verrucae ratings with an inter-rater reliability test to evaluate the strength of our ratings. Two raters evaluated verrucae size on gross photographs and assigned a rating within 1–5 on verrucae size protocol. A verrucae rating of "1" means a flat cortical surface and shows no verrucae while a verrucae rating of "5" signifies large verrucae present across the entorhinal surface. The raters utilized and referred to the same verrucae rating protocol described in the methods. Utilizing a Cohen's Kappa, we found agreement among the two raters (Kappa = 0.38, $p < 0.001$).

Verrucae size correlates with Braak and Braak stage

Next, we compared photographs and surface reconstructions in normal control (Fig. 6a, b) and Alzheimer's cases (Fig. 6c, d). We rated verrucae (based on qualitative protocol) and tested the verrucae ratings against pathological diagnosis. We confirmed that the MRI reconstructions represented the verrucae precisely and provided validation for the gross or photographic surfaces. Our rating results corroborate our quantitative measurements described above where we quantified verrucae size in a subset of cases.

With a significant difference in quantitative verrucae measures between controls and mild AD samples, we next examined the pathological marker in AD. To assess pathological diagnosis, we stained for neurofibrillary tangles and amyloid plaques with thioflavine S and staged each case based on Braak and Braak criteria for neurofibrillary

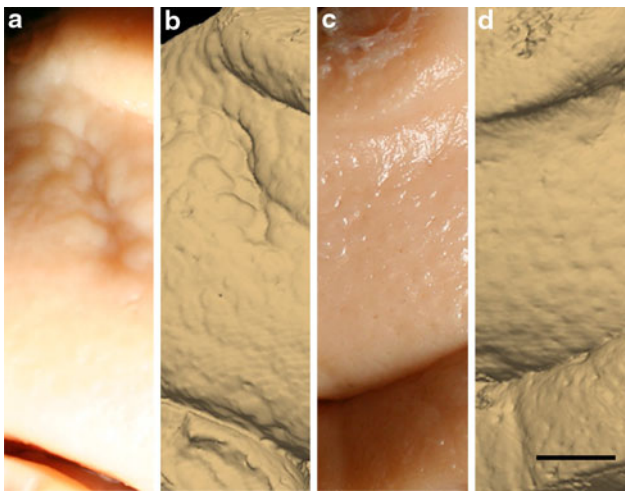

Fig. 6 Gross brain specimen shows entorhinal cortex surface in a control case (**a**), validated with the ex vivo MRI surface reconstruction in (**b**). Gross specimen of entorhinal cortex surface in a moderate Alzheimer's disease case (**c**), validated with the ex vivo MRI surface reconstruction in (**d**). Note the larger verrucae present in the control sample (**a** and **b**) compared with the Alzheimer's case (**c** and **d**). *Magnification bar* 0.25 cm

tangles and amyloid plaques. All Braak and Braak staging analyses were confirmed by Department of Neuropathology at MGH with anti-tau antibody or Bielschowsky's silver stain. We observed that most cases, even cognitively normal cases, contained a few isolated NFTs. Diagnosis and Braak and Braak stage are listed in Table 1. After staining and staging, we compared verrucae rating to Braak and Braak stage and found that verrucae ranking negatively correlated to Braak and Braak staging (Fig. 7) ($p < 0.01$, Spearman's $\rho = -0.526$, $n = 36$). Furthermore, we also found that verrucae ratings were significantly different when comparing normal controls to AD severity in increments. Normal controls had significantly higher ratings than Braak and Braak stage III and IV (Mann–Whitney U test, $p < 0.001$) and Braak and Braak stage V and VI (Mann–Whitney U test, $p < 0.001$). Verrucae ratings were not significantly different between normal controls and Braak and Braak stage I and II (Mann–Whitney U test, $p = 0.084$) but these groups showed a significantly difference in our quantitative results (height, volume, width and surface area) with mild AD cases decreased compared to controls.

Age, gender, post mortem interval and fixative

Within the normal control group, we did not observe a relationship between verrucae and age, gender, postmortem interval nor fixation in paraformaldehyde or formalin. Postmortem interval is the time that passes between death and time of fixation of the brain. It could be a concern that the verrucae collapse after death but we did not find that postmortem interval showed any relationship with the overall size of the verrucae (Spearman's $\rho = 0.274$, $p = 0.42$, $n = 11$). Among our cases, we found that no significant difference between male and female entorhinal cortices (Mann–Whitney U test, $p = 0.82$). We were unable to examine laterality with our sample set because we did not obtain both hemispheres. We scrutinized the samples to determine whether formalin or paraformaldehyde had an effect on verrucae size but did not observe a difference qualitatively. As described above, we observed a height difference in verrucae between normal controls and AD samples in our quantitative measurements that were all within the formalin-fixed group which precludes technical differences between fixatives. In addition, we did not observe any tissue differences between fixatives and all cases were well preserved. All cases sectioned and stained properly and nothing remarkable was observed in MRI or histology concerning fixation.

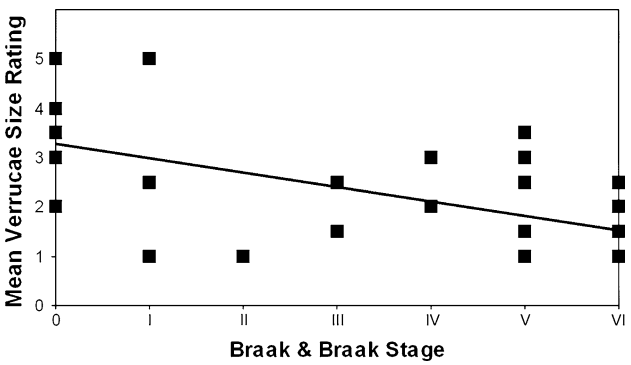

Fig. 7 Mean verrucae size ratings were significantly negatively correlated (Spearman's $\rho = -0.526$, $p < 0.01$, $n = 36$) with Braak and Braak stage

Discussion

In a previous study, we demonstrated that layer II islands are visible in the entorhinal cortex using ex vivo MRI [4] and that these islands could be used to localize entorhinal cortex in vivo [18]. Here, we built on this model, and created entorhinal surface reconstructions to quantify spatial and morphometric properties of the verrucae. Utilizing ex vivo MRI, we confirmed that entorhinal islands colocalize with entorhinal verrucae, i.e., that each island is beneath a verruca, as originally detailed previous neuroanatomical studies [30, 40, 44, 54, 55]. We validated our model with qualitative assessment in the gross specimen and showed that verrucae measurements accurately reflect their true size. The validated models were then used to demonstrate that entorhinal surfaces in control cases differed significantly from other cortical regions. Finally, with this morphometric model, we determined that entorhinal verrucae in control cases were significantly larger than mild AD cases, and that verrucae size significantly and negatively correlated to Braak and Braak stage determined by NFTs in all stages.

The novelties of our study include unique application of imaging methods on entorhinal surface reconstructions (i.e., new model development), quantitative demonstration of individual verruca size (height, width, surface area and volume), establishment of verrucae ratings or grades (i.e., qualitative assessment of verrucae in control and Alzheimer's disease cases) and finally correlation of verrucae rating to Braak and Braak neurofibrillary tangle stages. No prior study has described individual verruca size quantitatively, or its correlation to AD severity and with high-resolution imaging methods.

Visible to the unaided eye, neuroanatomists described entorhinal verrucae a century ago [30, 40]. The human eye (20/20 vision) can resolve objects about 0.1 mm long which is consistent with our verrucae measurements of approximately 0.13 mm in height (mean) and 1.26 mm in width (mean) for control cases. In AD, however, verrucae

become atrophic and shrink, and are not observed in severe cases [44, 53, 55]. Our results confirm these findings, and demonstrate that a semi-automated model derived from neuroimaging data can provide a quantitative assessment of individual verrucae sensitive enough to detect and quantify AD-related atrophy even in its mildest stage.

We compared our findings from entorhinal cortex to neocortical and other limbic surfaces to demonstrate that the method utilized is specific to regions of the brain containing verrucae. The lack of height in neocortical areas demonstrates that our quantitative measures correspond to what can be observed visually. It is noteworthy that since our voxel size represents isotropic data at 100 μm^3 and since verrucae means were 0.13 and 1.26 mm for control cases, each verrucae measurement symbolizes several ($\sim$13) voxels in width and at minimum 1 voxel in height. In our mild AD cases, verrucae width (mean) was 1.14 mm and height was 0.11 mm and contained several ($\sim$11) voxels in width and at minimum 1 voxel in height. Given this relationship and high resolution, we avoid partial voluming issues even in mild AD cases as quantitative measurements were not performed on severe cases.

Prior work has examined entorhinal verrucae. Our data demonstrate a decrease in verrucae size with a disease process (Alzheimer's disease) whereas the Simic and colleagues [43] examined normal aging. These two studies examined different matters. The extensive study by Simic which used molded casts reported the total number of verrucae on the surface, overall entorhinal surface area and counted neurons in non-demented aging. Our study quantified the size of individual verrucae (height, width, volume and surface area) and compared the size to Alzheimer diagnosis and severity (Braak and Braak stage). Additionally, the prior study examined a sample of tissue spanning a wide range of adult life from age 23 to 85 and found 60 cases had neither cognitive impairment (i.e., normal controls and/or normal aging) nor neurological incident. In the current study, NFTs were correlated with verrucae morphology. It could be postulated that verrucae increase in total number during aging from cross-sectional data [43] but once the Alzheimer's cascade begins, then the verrucae decrease in size and eventually disappear due to neuronal loss that gives way to neurofibrillary tangles. Alternatively, Simic and colleagues suggested that verrucae may split into smaller verrucae and that may account for the increase in total number of verrucae during aging. With regard to normal aging, the Simic study remains the most significant report to date cataloging the number of verrucae as a function of age, and has provided the best examination of verrucae in younger persons and healthy older adults with most of their samples gifted from individuals without neurodegenerative diseases. Our study further characterized the verrucae trajectory in Alzheimer's disease and showed differences in verrucae size, suggesting that verrucae height and volume were the most affected in our AD samples and related to disease severity. We further showed that all verrucae measures were significantly different in mild AD compared to normal controls. Taken together, these results begin to establish the normal architecture and magnitude of the verrucae in healthy aging and AD.

We speculate that the mechanisms that account for the reduction of verrucae are neuronal loss, neuronal shrinkage due to neurofibrillary tangles and/or decreased synaptic connections in entorhinal cortex layer II. Neurofibrillary tangles are typically smaller in size than a functioning healthy neuron [28, 33–35] so that decrease could account for the decrease in verrucae size we observed in AD. Neuronal diameter measurements have been reported in AD where decreased neuronal diameter was demonstrated in AD compared to controls and that neuronal size was 30% smaller in neurons with neurofibrillary tangles [34, 35]. Decreased neuronal measurements have also been observed in the aging brain in neocortical areas, especially frontal and temporal areas [48, 49]. It is important to note that that the presence of a neurofibrillary tangle means that a neuron has died [56] and that neurofibrillary tangles indicate neuronal loss [5, 21]. Age-related and Alzheimer's-related neuronal loss has been reported [20, 21, 25, 26, 32, 43, 48], but future studies will have to determine whether or not verrucae size relates to stereologically defined neuronal loss. Since Braak and Braak [10] staging is based on the presence of neurofibrillary tangles in the medial temporal lobe and given the fact that neurofibrillary tangles have been strongly correlated to clinical dementia by several groups [2, 9, 19, 21, 32] and in large sample studies [41], we consider using Braak and Braak staging to assess the severity of cases the closest pathological metric to cognitive behavior. There is little doubt that the presence of neurofibrillary tangles, more than a few isolated tangles, signifies the person has memory impairment [36]. Synaptic degeneration is also a variable in AD and several studies have demonstrated decreases in the number of synapses [1, 37, 47], and decreases in synaptic proteins (i.e., synaptophysin) [11, 24, 45] in hippocampus and entorhinal cortex in AD, notably early in disease progression. Some evidence suggests that decreases in synaptic density occur after age 65 [38] and others have demonstrated a correlation between dystrophic neurites and severity of dementia [6, 45]. Even so, neuronal cell death is likely the principal basis for the reduction in verrucae size with a smaller contribution due to other mechanisms such as synaptic degeneration. It is possible that collectively these mechanisms may be responsible for the reduction in verrucae size in AD.

Given that cases with large verrucae were less likely to have AD, our results beg the question; do large verrucae

represent cognitive resilience and healthy aging? It is unquestionable that cognitive resilience, or cognitively normal cases with AD pathological changes, is an existing, albeit small, category in neuropathology [8, 15, 17, 23, 39, 42]. Even in cognitively normal cases, most of our cases contained a few NFTs and this was consistent with existing studies that have described NFTs in aging [3, 23, 31]. The density of NFTs and decreased neuronal numbers remain reliable correlates that predict dementia [2, 19, 20, 26]. Our results suggest that verrucae height measures below 0.12 mm predict a mild AD diagnosis. Given that we observed the largest height in an individual verrucae was 0.25 mm and that verrucae in mild AD cases were typically below 0.12 mm and that flat cortex is less than 0.10 mm, a quantitative range exists that may correspond to cognitively healthy aging and mild cognitive impairment. Variability in neurofibrillary tangles, early in the disease, has been reported in Alzheimer's disease [22]. Currently, it is unknown what accounts for this variability in verrucae size. This may be explained by cognitive resilience where variation in verrucae size across cases may account for categorical groups: AD (Alzheimer's dementia), frail (dementia without neuropathological markers), cognitive resilience (no clinical dementia but with neuropathological markers), and normal controls (cognitively normal and no pathological markers). Future studies will have to establish these relationships with cognitive and behavioral data. Nonetheless, the characterization of verrucae not only contributes to understanding a biological phenomenon but also establishes verrucae absence as a metric for earlier AD diagnosis and may provide initial evidence for the future cognitive resilience hypotheses.

While the resolution used here is not achievable using current clinical in vivo technology, further characterization of verrucae with ex vivo methods allows us to define the neural correlates of this unique structure, and examine the variability between individuals. Verrucae detection will require isotropic voxels that will challenge neuroimaging technologies as structures require 3D assessment. Nevertheless, neuroimaging continually improves resolution and acquisition techniques such as motion correction or phase imaging that may advance avenues of early detection [16, 50]. Most importantly, the correlation of histology and ex vivo MR imaging provides a tool for validation with many proteins, neurons and pathological states and these results offer a bridge to applying these tools to in vivo imaging when available.

In summary, our data indicate that verrucae changes, particularly in height and volume, may reflect the pathological presence of NFTs (i.e., neuronal loss) and provide a morphological marker to diagnose AD. Entorhinal verrucae represent a highly specific structural marker for detecting AD early in the course of the disease, and provide a potentially sensitive marker for future neuroimaging. The capacity to determine localized changes in relation to pathology may have considerable repercussions in terms of clinical diagnosis of AD and the future applications of this technique could identify changes in other disorders as well.

Acknowledgments We would like to thank those who donated tissue; their generous donation made this work possible. We also thank David Salat for comments and discussion. Support for this research was provided in part by the National Center for Research Resources (P41-RR14075, and the NCRR BIRN Morphometric Project BIRN002, U24 RR021382), the National Institute for Biomedical Imaging and Bioengineering (R01EB006758), the National Institute on Aging (AG022381) and (AG028521), the National Center for Alternative Medicine (RC1AT005728-01), the National Institute for Neurological Disorders and Stroke (R01 NS052585-01, 1R21NS072652-01, 1R01NS070963), and was made possible by the resources provided by Shared Instrumentation Grants 1S10RR023401, 1S10RR019307, and 1S10RR023043. Additional support was provided by The Autism and Dyslexia Project funded by the Ellison Medical Foundation and by the NIH Blueprint for Neuro-science Research (U01-MH093765, part of the multi-institutional Human Connectome Project).

References

1. Arendt T (2009) Synaptic degeneration in Alzheimer's disease. Acta Neuropathol 118:167–179
2. Arriagada PV, Growdon JH, Hedley-Whyte ET, Hyman BT (1992) Neurofibrillary tangles but not senile plaques parallel duration and severity of Alzheimer's disease. Neurology 42:631–639
3. Arriagada PV, Marzloff K, Hyman BT (1992) Distribution of Alzheimer-type pathologic changes in nondemented elderly individuals matches the pattern in Alzheimer's disease. Neurology 42:1681–1688
4. Augustinack JC, van der Kouwe AJ, Blackwell ML, Salat DH, Wiggins CJ, Frosch MP, Wiggins GC, Potthast A, Wald LL, Fischl BR (2005) Detection of entorhinal layer II using 7 Tesla magnetic resonance imaging. Ann Neurol 57:489–494
5. Ball MJ (1977) Neuronal loss, neurofibrillary tangles and granulovacuolar degeneration in the hippocampus with ageing and dementia. A quantitative study. Acta Neuropathol 37:111–118
6. Bancher C, Jellinger K, Lassmann H, Fischer P, Leblhuber F (1996) Correlations between mental state and quantitative neuropathology in the Vienna Longitudinal Study on Dementia. Eur Arch Psychiatry Clin Neurosci 246:137–146
7. Barbier EL, Marrett S, Danek A, Vortmeyer A, van Gelderen P, Duyn J, Bandettini P, Grafman J, Koretsky AP (2002) Imaging cortical anatomy by high-resolution MR at 3.0 T: detection of the stripe of Gennari in visual area 17. Magn Reson Med 48:735–738
8. Bennett DA, Schneider JA, Arvanitakis Z, Kelly JF, Aggarwal NT, Shah RC, Wilson RS (2006) Neuropathology of older persons without cognitive impairment from two community-based studies. Neurology 66:1837–1844
9. Bennett DA, Schneider JA, Bienias JL, Evans DA, Wilson RS (2005) Mild cognitive impairment is related to Alzheimer disease pathology and cerebral infarctions. Neurology 64:834–841
10. Braak H, Braak E (1991) Neuropathological staging of Alzheimer-related changes. Acta Neuropathol 82:239–259
11. Cabalka LM, Hyman BT, Goodlett CR, Ritchie TC, Van Hoesen GW (1992) Alteration in the pattern of nerve terminal protein immunoreactivity in the perforant pathway in Alzheimer's disease and in rats after entorhinal lesions. Neurobiol Aging 13:283–291

12. Cajal SR (1955) Studies on the cerebral cortex (translated from Spanish by Kraft LM). Yearbook Publishers, Chicago
13. Clark VP, Courchesne E, Grafe M (1992) In vivo myeloarchitectonic analysis of human striate and extrastriate cortex using magnetic resonance imaging. Cereb Cortex 2:417–424
14. Cline HE, Dumoulin CL, Hart HR Jr, Lorensen WE, Ludke S (1987) 3D reconstruction of the brain from magnetic resonance images using a connectivity algorithm. Magn Reson Imaging 5:345–352
15. Davis DG, Schmitt FA, Wekstein DR, Markesbery WR (1999) Alzheimer neuropathologic alterations in aged cognitively normal subjects. J Neuropathol Exp Neurol 58:376–388
16. Duyn JH, van Gelderen P, Li TQ, de Zwart JA, Koretsky AP, Fukunaga M (2007) High-field MRI of brain cortical substructure based on signal phase. Proc Natl Acad Sci USA 104:11796–11801
17. Ewbank DC, Arnold SE (2009) Cool with plaques and tangles. N Engl J Med 360:2357–2359
18. Fischl B, Stevens AA, Rajendran N, Yeo BT, Greve DN, Van Leemput K, Polimeni JR, Kakunoori S, Buckner RL, Pacheco J, Salat DH, Melcher J, Frosch MP, Hyman BT, Grant PE, Rosen BR, van der Kouwe AJ, Wiggins GC, Wald LL, Augustinack JC (2009) Predicting the location of entorhinal cortex from MRI. Neuroimage 47:8–17
19. Giannakopoulos P, Herrmann FR, Bussiere T, Bouras C, Kovari E, Perl DP, Morrison JH, Gold G, Hof PR (2003) Tangle and neuron numbers, but not amyloid load, predict cognitive status in Alzheimer's disease. Neurology 60:1495–1500
20. Gomez-Isla T, Hollister R, West H, Mui S, Growdon JH, Petersen RC, Parisi JE, Hyman BT (1997) Neuronal loss correlates with but exceeds neurofibrillary tangles in Alzheimer's disease. Ann Neurol 41:17–24
21. Gomez-Isla T, Price JL, McKeel DW Jr, Morris JC, Growdon JH, Hyman BT (1996) Profound loss of layer II entorhinal cortex neurons occurs in very mild Alzheimer's disease. J Neurosci 16:4491–4500
22. Hanke J, Yilmazer-Hanke DM (1997) Variabilities in the distribution of neurofibrillary tangles in the anterior parahippocampal gyrus at initial stages of Alzheimer's disease. Clin Neuropathol 16:299–302
23. Haroutunian V, Purohit DP, Perl DP, Marin D, Khan K, Lantz M, Davis KL, Mohs RC (1999) Neurofibrillary tangles in nondemented elderly subjects and mild Alzheimer disease. Arch Neurol 56:713–718
24. Heinonen O, Soininen H, Sorvari H, Kosunen O, Paljarvi L, Koivisto E, Riekkinen PJ Sr (1995) Loss of synaptophysin-like immunoreactivity in the hippocampal formation is an early phenomenon in Alzheimer's disease. Neuroscience 64:375–384
25. Heinsen H, Henn R, Eisenmenger W, Gotz M, Bohl J, Bethke B, Lockemann U, Puschel K (1994) Quantitative investigations on the human entorhinal area: left–right asymmetry and age-related changes. Anat Embryol 190:181–194
26. Hof PR, Bussiere T, Gold G, Kovari E, Giannakopoulos P, Bouras C, Perl DP, Morrison JH (2003) Stereologic evidence for persistence of viable neurons in layer II of the entorhinal cortex and the CA1 field in Alzheimer disease. J Neuropathol Exp Neurol 62:55–67
27. Hyman BT, Van Hoesen GW, Damasio AR, Barnes CL (1984) Alzheimer's disease: cell-specific pathology isolates the hippocampal formation. Science 225:1168–1170
28. Iqbal K, Wisniewski HM, Grundke-Iqbal I, Terry RD (1977) Neurofibrillary pathology: an update. In: Nandy K, Sherwin I (eds) The aging brain and senile dementia. Plenum, New York, pp 209–227
29. Kemper T (1984) Neuroanatomical and Neuropathological changes in normal aging and in dementia kemper. In: Albert ML, Knopefel JE (eds) Clinical neurology of aging. Oxford University Press, New York, pp 9–52
30. Klinger J. (1948) Die makroskopische Anatomie der Ammonsformation. Denkschr. Schweiz. Naturforsch 78
31. Knopman DS, Parisi JE, Salviati A, Floriach-Robert M, Boeve BF, Ivnik RJ, Smith GE, Dickson DW, Johnson KA, Petersen LE, McDonald WC, Braak H, Petersen RC (2003) Neuropathology of cognitively normal elderly. J Neuropathol Exp Neurol 62:1087–1095
32. Kordower JH, Chu Y, Stebbins GT, DeKosky ST, Cochran EJ, Bennett D, Mufson EJ (2001) Loss and atrophy of layer II entorhinal cortex neurons in elderly people with mild cognitive impairment. Ann Neurol 49:202–213
33. Mann DM, Neary D, Yates PO, Lincoln J, Snowden JS, Stanworth P (1981) Alterations in protein synthetic capability of nerve cells in Alzheimer's disease. J Neurol Neurosurg Psychiatry 44:97–102
34. Mann DM, Neary D, Yates PO, Lincoln J, Snowden JS, Stanworth P (1981) Neurofibrillary pathology and protein synthetic capability in nerve cells in Alzheimer's disease. Neuropathol Appl Neurobiol 7:37–47
35. Mann DM, Yates PO (1981) The relationship between formation of senile plaques and neurofibrillary tangles and changes in nerve cell metabolism in Alzheimer type dementia. Mech Ageing Dev 17:395–401
36. Markesbery WR (2010) Neuropathologic alterations in mild cognitive impairment: a review. J Alzheimers Dis 19:221–228
37. Marksteiner J, Kaufmann WA, Gurka P, Humpel C (2002) Synaptic proteins in Alzheimer's disease. J Mol Neurosci 18:53–63
38. Masliah E, Crews L, Hansen L (2006) Synaptic remodeling during aging and in Alzheimer's disease. J Alzheimers Dis 9:91–99
39. Nelson PT, Kukull WA, Frosch MP (2010) Thinking outside the box: Alzheimer-type neuropathology that does not map directly onto current consensus recommendations. J Neuropathol Exp Neurol 69:449–454
40. Retzius G (1896) Das Menschenhirn. Norstedt and Sonhe, Stockholm
41. Savva GM, Wharton SB, Ince PG, Forster G, Matthews FE, Brayne C (2009) Age, neuropathology, and dementia. N Engl J Med 360:2302–2309
42. Silver MH, Newell K, Brady C, Hedley-White ET, Perls TT (2002) Distinguishing between neurodegenerative disease and disease-free aging: correlating neuropsychological evaluations and neuropathological studies in centenarians. Psychosom Med 64:493–501
43. Simic G, Bexheti S, Kelovic Z, Kos M, Grbic K, Hof PR, Kostovic I (2005) Hemispheric asymmetry, modular variability and age-related changes in the human entorhinal cortex. Neuroscience 130:911–925
44. Solodkin A, Van Hoesen GW (1996) Entorhinal cortex modules of the human brain. J Comp Neurol 365:610–617
45. Sze CI, Troncoso JC, Kawas C, Mouton P, Price DL, Martin LJ (1997) Loss of the presynaptic vesicle protein synaptophysin in hippocampus correlates with cognitive decline in Alzheimer disease. J Neuropathol Exp Neurol 56:933–944
46. Terry RD. (1995) Biologic differences between early- and late-onset Alzheimer disease. Alzheimer Dis Assoc Dis 9(Suppl 1): S26–S27
47. Terry RD (2000) Cell death or synaptic loss in Alzheimer disease. J Neuropathol Exp Neurol 59:1118–1119
48. Terry RD, DeTeresa R, Hansen LA (1987) Neocortical cell counts in normal human adult aging. Ann Neurol 21:530–539
49. van de Nes JA, Nafe R, Schlote W (2008) Non-tau based neuronal degeneration in Alzheimer's disease–an immunocytochemical and quantitative study in the supragranular layers of the middle temporal neocortex. Brain Res 1213:152–165

50. van der Kouwe AJ, Benner T, Dale AM (2006) Real-time rigid body motion correction and shimming using cloverleaf navigators. Magn Reson Med 56:1019–1032
51. Van Hoesen G, Pandya DN (1975) Some connections of the entorhinal (area 28) and perirhinal (area 35) cortices of the rhesus monkey. I. Temporal lobe afferents. Brain Res 95:1–24
52. Van Hoesen GW (1995) Anatomy of the medial temporal lobe. Magn Reson Imaging 13:1047–1055
53. Van Hoesen GW, Augustinack JC, Dierking J, Redman SJ, Thangavel R (2000) The parahippocampal gyrus in Alzheimer's disease. Clinical and preclinical neuroanatomical correlates. Ann N Y Acad Sci 911:254–274
54. Van Hoesen GW, Hyman BT, Damasio AR (1991) Entorhinal cortex pathology in Alzheimer's disease. Hippocampus 1:1–8
55. Van Hoesen GW, Solodkin A (1993) Some modular features of temporal cortex in humans as revealed by pathological changes in Alzheimer's disease. Cereb Cortex 3:465–475
56. Wisniewski HM, Soifer D (1979) Neurofibrillary pathology: current status and research perspectives. Mech Ageing Dev 9:119–142